acylium ion **14C** which rapidly recyclizes to the product (+)-**15**. The facility with which this process occurs both in the cyclopentano annulation **10** and the cyclopropano annulation **15** bodes well for its synthetic utility.

To demonstrate that these in situ enamide alkylations to **10** and **15** are only part of the inherent interest in these systems, we were able to transform them into chiral, nonracemic carbocycles. Thus, treatment of **10** with methyllithium (−78 °C to −40 °C,

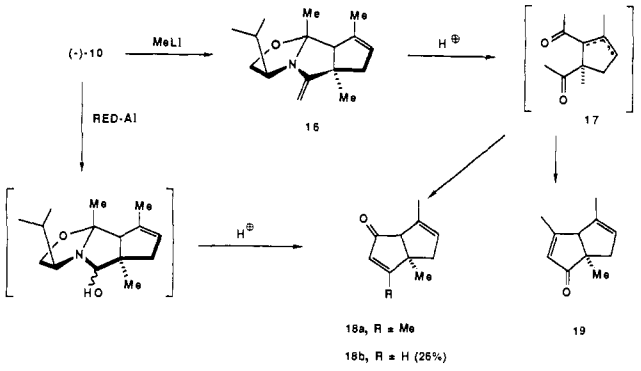

THF) gave the dehydrated addition product **16** and then directly hydrolyzed (EtOH–1 M $Bu_4NH_2PO_4$, 1:1, 80 °C, 24 h), via the diketone **17**, to a 5:1 mixture of the novel chiral cyclopentenones **18a** ($[\alpha]^{22}_D$ 62.2°, *c* 0.6, $CHCl_3$) and **19** which were readily separated (SiO_2, Et_2O–Hex, 1:10). If (−)-**10** is reduced with RED-Al, the resulting carbinol amine is formed, which was hydrolyzed as above to the chiral cyclopentenone **18b**, along with 52% of the keto aldehyde precursor.[8] In a related manner, the cyclopropane derivative (+)-**15** could also be transformed into

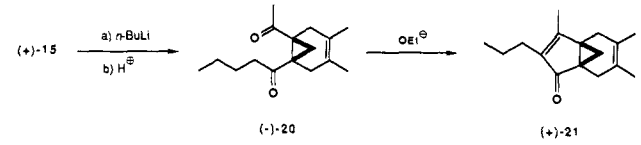

a novel carbocycle. Addition of *n*-butyllithium to **15** gave the butylcarbinol adduct which, without isolation, was directly hydrolyzed (EtOH–1 M $Bu_4NH_2PO_4$, 4:1 80 °C, 5 h) to the diketone (−)-**20** in 98% yield for both steps. Base-catalyzed aldolization (NaOEt, EtOH, 24 h, 25 °C) produced the tricyclic ketone (+)-**21** (91%, $[\alpha]_D$ 48.0°, *c* 0.40, acetone).

This study is continuing with a wide variety of substrates and with an eye toward reaching unusual carbocyclic frameworks of both natural and unnatural substances.

Acknowledgment. We are grateful to the National Institutes of Health and the National Science Foundation for financial support of this work. A fellowship (to St.B.) from the Schweizerische Nationalfonds zur Förderung der Wissenschaftlichen Forschung is also gratefully acknowledged.

Supplementary Material Available: Synthesis, analytical data, and spectral data (^1H NMR; ^{13}C NMR, IR, and MS) for all compounds (17 pages). Ordering information is given on any current masthead page.

(8) Support for the structural assignment of **18a** and **19** is gained from the spectral properties of **18b**. The latter shows proton chemical shifts very smilar to **18a**. Since the precursor to **18b** is the keto-aldehyde **C**, it can only cyclize in the manner shown. The isomer **19** is quite different showing angular H at 3.15, angular methyl 1.25, and vinyl methyl at 1.86.

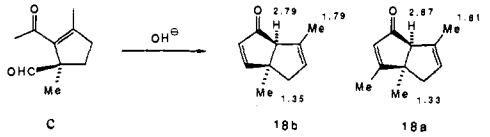

Structural and Electronic Consequences of Protonation in $\{Mn_4O_6\}^{4+}$ Cores: pH Dependent Properties of Oxo-Bridged Manganese Complexes

Karl S. Hagen, T. David Westmoreland, Michael J. Scott, and William H. Armstrong*

Department of Chemistry, University of California Berkeley, California 94720

Received August 22, 1988

Recognition that the oxygen-evolving complex of photosystem II (PSII) employs two to four manganese atoms to carry out catalytic water oxidation[1] has engendered interest in preparing synthetic models for this active site.[2] It is generally thought that ligands derived from water (O^{2-} or OH^-) are present as bridges between manganese atoms in the catalytic site. While a variety of oxo-bridged polynuclear manganese complexes has been characterized,[2] very few hydroxo-bridged species have been reported.[3] In the course of recent studies[2a] aimed at preparing polynuclear manganese complexes, we have discovered a synthetic route which affords the novel mixed oxo/hydroxo-bridged tetranuclear Mn(IV) complex, $[Mn_4O_5(OH)(tame)_4](CF_3SO_3)_5$,[4] $\mathbf{1}(CF_3SO_3)_5$. This compound contains a protonated form of the $\{Mn_4O_6\}^{4+}$ core, also found in $[Mn_4O_6(tacn)_4]^{4+}$.[5] The adamantane-shaped $\{Mn_4O_6\}^{4+}$ core has been proposed as a reaction intermediate in photosynthetic water oxidation.[6] As magnetic measurements have been used extensively to characterize the oxygen-evolving complex, structural and magnetic properties due to protonation of this tetranuclear core are of particular interest.

Compound $\mathbf{1}(CF_3SO_3)_5$ was isolated in approximately 30% yield from a 1:1:3 acetonitrile solution of tame·$3CF_3SO_3H$, $Mn(CF_3SO_3)_2$·MeCN, and Et_3N after exposure to atmospheric O_2 for 36 h. Material suitable for elemental analysis[7] and X-ray diffraction experiments[8] was obtained directly from the reaction mixture. The cluster can be deprotonated by treatment with Et_3N in CH_3CN to give $[Mn_4O_6(tame)_4]^{4+}$ (**2**), which has a visible spectrum[9] very similar to that of $[Mn_4O_6(tacn)_4]^{4+}$ (**3**). For

(1) (a) Brudvig, G. W. In *Metal Clusters in Proteins*; Que, L., Jr., Ed.; ACS Symposium Series 372; American Chemical Society: Washington, DC, 1988; pp 221–237. (b) Pecoraro, V. L. *Photochem. Photobiol.* **1988**, *48*, 249–264. (c) Babcock, G. T. In *New Comprehensive Biochemistry: Photosynthesis*; Amesz, T., Ed.; Elsevier: Amsterdam, 1987; pp 125–158. (d) Dismukes, G. *Photochem. Photobiol.* **1986**, *43*, 89–115. (e) Govindjee; Karmbara, T.; Coleman, W. *Photochem. Photobiol.* **1985**, *42*, 187–210.

(2) Selected examples: (a) Hagen, K. S.; Armstrong, W. H.; Hope, H. *Inorg. Chem.* **1988**, *27*, 967–969. (b) Hagen, K. S.; Armstrong, W. H.; Olmstead, M. M. *J. Am. Chem. Soc.* **1989**, *111*, 774–775. (c) Christou, G.; Vincent, J. B. In *Metal Clusters in Proteins*; Que, L., Jr., Ed.; ACS Symposium Series 372; American Chemical Society: Washington, DC, 1988; pp 238–255. (d) Towle, D. K.; Botsford, C. A.; Hodgson, D. J. *Inorg. Chim. Acta* **1988**, *141*, 167–168. (e) Stebler, M.; Ludi, A.; Bürgi, H.-B. *Inorg. Chem.* **1986**, *25*, 4743–4750. (f) Mênage, S.; Girerd, J.-J.; Gleizes, A. *J. Chem. Soc., Chem. Commun.* **1988**, 431–432. (g) Suzuki, M.; Tokura, S.; Suhara, M.; Uehara, A. *Chem. Lett.* **1988**, 477–480.

(3) (a) Maslen, H. S.; Waters, T. N. *J. Chem. Soc., Chem. Commun.* **1973**, 760–761. (b) Boucher, L. J.; Coe, C. G. *Inorg. Chem.* **1976**, *15*, 1334–1340.

(4) Abbreviations used: tacn = 1,4,7-triazacyclononane, $HNCH_2CH_2NHCH_2CH_2NHCH_2CH_2$; tame = 1,1,1-tris(aminomethyl)ethane, $H_3CC(CH_2NH_2)_3$; PSII = photosystem II.

(5) (a) Wieghardt, K.; Bossek, U.; Gebert, W. *Angew. Chem., Int. Ed. Engl.* **1983**, *22*, 328–329. (b) Wieghardt, K.; Bossek, U.; Nuber, B.; Weiss, J.; Bonvoisin, J.; Corbella, M.; Vitolis, S. E.; Girerd, J.-J. *J. Am. Chem. Soc.* **1988**, *110*, 7398–7411.

(6) Brudvig, G. W.; Crabtree, R. H. *Proc. Natl. Acad. Sci. U.S.A.* **1986**, *83*, 4586–4588.

(7) Anal. Calcd for $C_{25}H_{61}F_{15}Mn_4N_{12}O_{21}S_5$: C, 19.61; H, 4.02; N, 10.98; S, 10.47. Found: C, 19.68; H, 3.95; N, 10.86; S, 10.56.

(8) X-ray analysis of $\mathbf{1}(CF_3SO_3)_5$. This complex crystallizes in the tetragonal space group $I4_1/a$, with a = 20.935 (3) Å, c = 13.084 (2) Å, V = 5735 Å^3, ρ_{calcd} = 1.773 g cm^{-3}, Z = 4. Data collection at 295 K out to 2θ = 45° afforded 1394 reflections with $I > 3\sigma(I)$. The structure was solved by direct methods and refined by using 200 parameters to final R (R_w) values of 5.47% (7.48%).

0002-7863/89/1511-1907$01.50/0

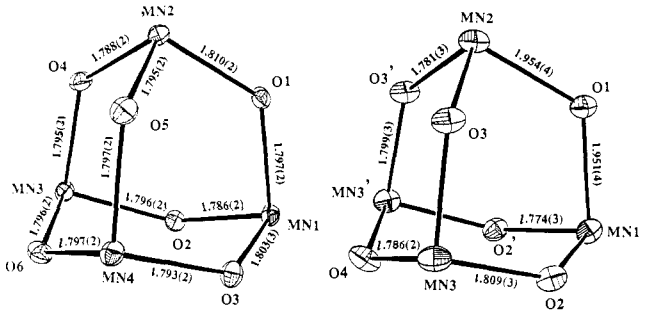

Figure 1. Left: Core structure of $[Mn_4O_6(tacn)_4]^{4+}$ (**3**), showing anisotropic thermal parameters, atom labeling scheme, and Mn–O bond distances. Additional interatomic distances (Å) and angles (deg): Mn(1)–Mn(2) 3.234 (1), Mn(1)–Mn(3) 3.226 (1), Mn(1)–Mn(4) 3.232 (1), Mn(2)–Mn(3) 3.216 (1), Mn(2)–Mn(4) 3.221 (1), Mn(3)–Mn(4) 3.230 (1), O(1)–Mn(1)–O(2) 98.4 (1), O(1)–Mn(1)–O(3) 98.6 (1), O(2)–Mn(1)–O(3) 99.3 (1), O(1)–Mn(2)–O(4) 99.1 (1), O(1)–Mn(2)–O(5) 99.1 (1), O(4)–Mn(2)–O(5) 99.5 (1), O(2)–Mn(3)–O(4) 98.8 (1), O(2)–Mn(3)–O(6) 98.7 (1), O(4)–Mn(3)–O(6) 98.9 (1), O(3)–Mn(4)–O(5) 98.8 (1), O(3)–Mn(4)–O(6) 98.8 (1), O(5)–Mn(4)–O(6) 99.1 (1), range for Mn–O–Mn angles: 127.40–128.5. Right: Core structure of $[Mn_4O_5(OH)(tacn)_4]^{5+}$ (**4**). Additional interatomic distances and angles: Mn(1)–Mn(2) 3.452 (1), Mn(1)–Mn(3) 3.259 (1), Mn(2)–Mn(3) 3.253 (1), Mn(3)–Mn(3′) 3.227 (1), O(1)–Mn(1)–O(2) 95.42 (1), O(2)–Mn–O(2′) 100.7 (2), O(1)–Mn(2)–O(3) 95.7 (1), O(3)–Mn(2)–O(3′) 100.5 (2), O(2)–Mn(3)–O(3) 97.2 (1), O(2)–Mn(3)–O(4) 98.5 (2), O(3)–Mn(3)–O(4) 99.2 (2), Mn(1)–O(1)–Mn(2) 124.2 (2), Mn(1)–O(2)–Mn(3) 130.9 (2), Mn(2)–O(3)–Mn(3) 130.7 (2), Mn(3)–O(4)–Mn(3′) 129.2 (2).

purposes of comparison, the protonated form of **3** was also synthesized. Addition of 70% aqueous $HClO_4$ to a CH_3CN solution of $[Mn_4O_6(tacn)_4](CF_3SO_3)_4$[10] afforded crystalline $[Mn_4O_5(OH)(tacn)_4](ClO_4)_5$, $\mathbf{4}(ClO_4)_5$, in nearly quantitative yield. Both $\mathbf{3}(ClO_4)_4$[11] and $\mathbf{4}(ClO_4)_5$[12] have been characterized by X-ray structural analysis. In both H_2O and CH_3CN protonation appears to be completely reversible, and a spectrophotometrically monitored titration of $\mathbf{3}(CF_3SO_4)_4$ in H_2O gave a pK_a of 3.50 ± 0.01.

In the solid-state structure of $\mathbf{1}(CF_3SO_3)_5$, the cation is positioned on an S_4 crystallographic axis, so that the OH group is disordered among four equivalent positions. However, the ClO_4^- salt of **4** crystallizes with the tetranuclear aggregate on a crystallographic mirror plane with no evidence of disorder (Figure 1). Although the proton position was not obtained from final difference Fourier maps, the bond distances indicate that O(1), which lies on the mirror plane, is unique and corresponds to the bridging hydroxide group, while the remaining oxygen bridges are oxo groups. In **4**, the average Mn–OH distance (1.953 Å) is 0.163 Å longer than the average Mn–O separation of 1.790 Å. By comparison, the average Mn–O bond distance in $\mathbf{3}(ClO_4)_4$ (Figure 1) is 1.796 Å, comparable to the corresponding values for $\mathbf{3}(Br)_4$[5] and $\mathbf{4}(ClO_4)_5$. Changes of this magnitude in bond lengths have been observed upon protonation of an oxo-bridged diiron species.[13] While the $\{Mn_4O_6\}^{4+}$ unit in $\mathbf{3}(ClO_4)_4$ rests on a general position, its point symmetry is nearly T_d. Protonation lowers the symmetry to approximately C_{2v} in $\mathbf{4}(ClO_4)_5$, although only C_s point symmetry is crystallographically required.

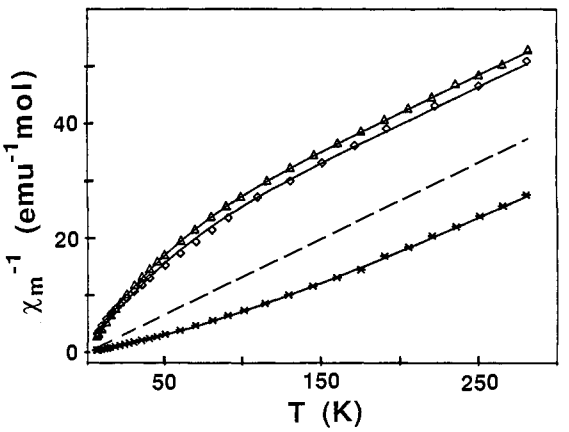

Figure 2. Inverse molar susceptibility per complex as a function of temperature for $\mathbf{1}(CF_3SO_3)_5$, ◇; $\mathbf{3}(ClO_4)_4$, *; and $\mathbf{4}(ClO_4)_5$, △. The data are corrected for the background contribution of the container and the diamagnetic contribution as calculated from Pascal's constants. The solid lines are generated from the fit parameters given in the text. The dashed line is the calculated Curie dependence for four uncoupled ($J = 0$) $S = 3/2$ ions.

Protonation of the $\{Mn_4O_6\}^{4+}$ core causes a dramatic change in its magnetic properties. For example, plots of $1/\chi$ vs T (Figure 2) demonstrate that the four d^3 Mn(IV) ions are ferromagnetically coupled in $\mathbf{3}(ClO_4)_4$, but in $\mathbf{1}(CF_3SO_3)_5$ and $\mathbf{4}(ClO_4)_5$ the net interaction is antiferromagnetic. The susceptibilities for the complexes were fit to an exchange hamiltonian $H_{ex} = \sum_{i>j} - J_{ij}S_i \cdot S_j$. For $\mathbf{3}(ClO_4)_4$, idealized tetrahedral symmetry of the four $S = {}^3/_2$ ions was assumed, and the best fit was obtained with $J = 14.5 \pm 0.3$ cm^{-1}. The quality of the fit was substantially improved by using the second-order hamiltonian $H_{ex} = -J\sum_{i>j} S_i \cdot S_j + j\sum_{i>j}(S_i \cdot S_j)^2$, $J = 13.85 \pm 0.09$ cm^{-1} and $j = 7.8 \pm 0.4$ cm^{-1}, giving the fit shown in Figure 2.[14] For the tetrahedral array, the eigenvalues and state degeneracies used were those given by Griffith.[15] As noted above, protonation of **3** reduces the core point symmetry to C_{2v} so that three independent J values are allowed. The best least-squares fit to the expression derived from the first-order exchange hamiltonian was obtained with $J_{12} = -39.6 \pm 0.1$ cm^{-1}, $J_{34} = 2.5 \pm 0.3$ cm^{-1}, J_{23} ($= J_{24} = J_{13} = J_{14}$) $= -19.6 \pm 0.1$ cm^{-1} for $\mathbf{1}(CF_3SO_3)_5$ and $J_{12} = -45 \pm 1.7$ cm^{-1}, $J_{34} = -2.7 \pm 0.2$ cm^{-1}, $J_{23} = -13.1 \pm 0.3$ cm^{-1} for $\mathbf{4}(ClO_4)_5$. Thus both protonated cores exhibit considerable net antiferromagnetic coupling in contrast to the ferromagnetic interactions in the deprotonated form. This observation is further confirmed by the moments per Mn ion at 280 K: $\mathbf{1}(CF_3SO_3)_5$, $\mu_{eff}/Mn = 3.26\ \mu_B$; $\mathbf{3}(CF_3SO_3)_4$, $\mu_{eff/Mn} = 4.51\ \mu_B$; $\mathbf{4}(ClO_4)_5$, $\mu_{eff/Mn} = 3.31\ \mu_B$; $S = {}^3/_2$ ion, $\mu_{eff} = 3.87\ \mu_B$.

Recent susceptibility measurements[16] of the difference between the S_1 and S_2 states of the oxygen-evolving complex of PSII show that $\mu_{S_2}^2 - \mu_{S_1}^2 = 17\ \mu_B^2$, and it has been suggested that this increase in μ^2 is consistent with a structural rearrangement accompanying oxidation. The results presented above and in Figure 2 additionally demonstrate the critical importance of protonation state in defining the magnetic properties of the $\{Mn_4O_6\}^{4+}$ core. For example, the $\Delta\mu^2$ value accompanying deprotonation discussed above $\mu_3^2 - \mu_4^2 = 37.19\ \mu_B^2$ at 280 K is only somewhat greater in magnitude than that observed for the $S_1 \rightarrow S_2$ transition in PSII. Attempts to interpret the magnetic properties of the oxygen-evolving complex in a given S state and the differences accompanying S-state changes must therefore consider changes in protonation of water-derived bridging ligands. Further studies directed toward examining the effects of bridge protonation on

(9) Electronic spectrum of **2** generated from **1** $(CF_3SO_3)_5$ by addition of Et_3N in CH_3CN: $\lambda_{max} = 549$ nm ($\epsilon = 2.4 \times 10^3$ M^{-1} cm^{-1}), 327 (sh, 1.7×10^4 M^{-1} cm^{-1}). Literature value[5b] for $\mathbf{3}(Br_4)\cdot 5.5H_2O$: $\lambda = 552$ ($\epsilon = 2.9 \times 10^3$ M^{-1} cm^{-1}), $\lambda = 336$ ($\epsilon = 1.7 \times 10^4$ M^{-1} cm^{-1}).

(10) $[Mn_4O_6(tacn)_4](CF_3SO_3)_4$ was generated by air oxidation of an acetonitrile solution containing 1:1 $Mn(CF_3SO_3)_2\cdot CH_3CN$:tacn and isolated as crystals by slow evaporation of solvent.

(11) X-ray analysis of $\mathbf{3}(ClO_4)_4$: This complex crystallizes in the monoclinic space group $C2/c$, with $a = 36.407$ (6) Å, $b = 11.282$ (1) Å, $c = 23.998$ (6) Å, $\beta = 91.23$ (2)°, $V = 9855$ Å^3, $\rho_{calcd} = 1.723$ g cm^{-3}, $Z = 8$. Data collection at 163 K out to $2\theta = 45°$ provided 4752 reflections with $I > 3\sigma(I)$. The structure was solved by direct methods and refined by using 625 parameters to final R (R_w) values of 3.96% (5.27%).

(12) X-ray analysis of $\mathbf{4}(ClO_4)_5\cdot 3CH_3CN$: This protonated complex crystallizes in the cubic space group $Im3$, with $a = 32.85$ (1) Å, $V = 35448$ Å^3, $\rho_{calcd} = 1.596$ g cm^{-1}, and $Z = 24$. Data collection at 153 K provided 3014 reflections with $I > 3\sigma(I)$. The structure was solved by direct methods and refined by using 374 parameters to R (R_w) values of 7.51% (10.21%).

(13) Armstrong, W. H.; Lippard, S. J. *J. Am. Chem. Soc.* **1984**, *106*, 4632–4633.

(14) The unusually large j/J ratio may be due to the neglect in the fits of zero field splitting in the $S = 6$ ground state.

(15) Griffith, J. S. *Mol. Phys.* **1972**, *24*, 833–842.

(16) Sivaraja, M.; Philo, J. S.; Lary, J.; Dismukes, G. C. *J. Am. Chem. Soc.*, in press.

structural and magnetic properties and the reactivity of oxo-bridged Mn aggregates are underway.

Acknowledgment. The authors gratefully acknowledge Professors K. Wieghardt, C. Dismukes, and J. Philo for preprints of work prior to publication. This work was supported by Grant No GM 382751-01 from the National Institute of General Medical Sciences.

Registry No. $1(CF_3SO_3)_5$, 118831-88-2; $2(CF_3SO_3)_4$, 118831-90-6; $3(CF_3SO_3)_4$, 118867-65-5; $3(ClO_4)_4$, 118867-62-2; $4(ClO_4)_5 \cdot 3CH_3CN$, 118867-64-4.

Supplementary Material Available: For each of $1(CF_3SO_3)_5$, $4(ClO_4)_5$, and $3(ClO_4)_4$ a fully labeled ORTEP drawing and tables of interatomic distances, interatomic angles, positional and isotropic equivalent thermal parameters, anisotropic thermal parameters, and molar susceptibility data (27 pages). Ordering information is given on any current masthead page.

Trimethyl Phosphite Traps Intermediates in the Reaction of $^1O_2$ and Diethyl Sulfide

Keepyung Nahm and Christopher S. Foote*

Department of Chemistry and Biochemistry
University of California
Los Angeles, California 90024
Received November 28, 1988

A variety of intermediates in $^1O_2$ reactions (ene reaction, 1,2-dioxetane, and endoperoxide formation) have been proposed as a result of studies of solvent and isotope effects and theoretical calculations.[1] The proposed intermediates have been trapped in a few cases.[2-6] Diphenyl sulfide and diphenyl sulfoxide have been used to trap intermediates in the reaction of $^1O_2$ with diethyl sulfide,[2] and methyl phenyl sulfoxide has been used to trap the intermediate in the reaction of $^1O_2$ with adamantylidene adamantane.[4] We report that trimethyl phosphite is surprisingly unreactive toward $^1O_2$ but very efficient in trapping the intermediate in the photooxidation of Et_2S.

Trimethyl phosphite has been used as a powerful reducing agent for peroxides,[7] but to our knowledge there has been no report of its use as to trap intermediates in photooxidation. We chose the reaction of Et_2S with $^1O_2$ because it is relatively well understood.[2,3,8] The rate constants for $^1O_2$ quenching by $(MeO)_3P$ and Et_2S were measured by $^1O_2$ emission (1270 nm) in various solvents (see Table I);[9] Figure 1 shows a typical plot from the $^1O_2$ emission

Table I. Rate Constants of $^1O_2$ Quenching by $(MeO)_3P$ and Sulfides[a]

quencher	methanol	acetonitrile	benzene	acetone	C_6H_6/MeOH[b]
$(MeO)_3P$	2.7×10^4[c]	6.6×10^4	4.7×10^4	6.3×10^4	3.9×10^4[d]
Et_2S	1.7×10^7	2.1×10^7[e]	2.0×10^7[e]		
PhSPh	$\sim 1.0 \times 10^5$[e]				

[a] M^{-1} s^{-1}. [b] 4:1 (v/v). [c] Methanol-OD. [d] 1.5×10^7 M^{-1} s^{-1} from ref 11. [e] Reference 8c.

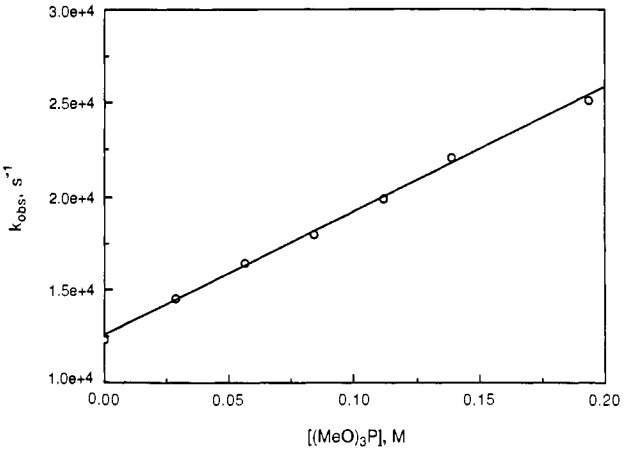

Figure 1. Singlet oxygen quenching by $(MeO)_3P$ in acetonitrile. The plot of k_{obsd} vs $[(MeO)_3P]$ has slope = quenching rate constant and intercept = singlet oxygen decay rate constant in the pure solvent: slope = 6.6×10^4 M^{-1} s^{-1}, intercept = 1.25×10^4 s^{-1}.

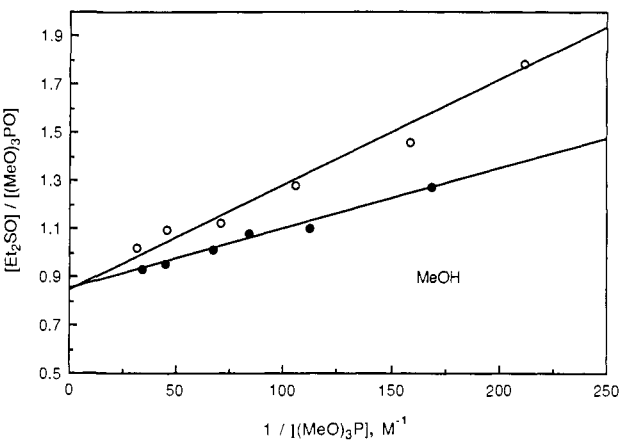

Figure 2. $(MeO)_3P$ trapping of Et_2S intermediate in MeOH: (○) 0.10 M Et_2S, slope = 0.0025(●), 0.20 M Et_2S, slope = 0.0044.

Scheme I

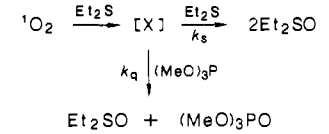

Scheme II

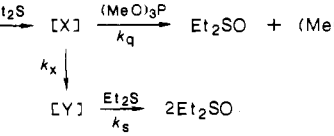

study. The slope is equal to the bimolecular quenching rate constant. The rates of quenching by Et_2S are at least 300 times faster than those by $(MeO)_3P$. A trap for intermediates must be relatively inert toward $^1O_2$ but reactive to the intermediates; from Table I, $(MeO)_3P$ satisfies the first condition. The rate constants for $(MeO)_3P$ ($2.7-6.6 \times 10^4$ M^{-1} s^{-1}) are far lower than those reported by Goe et al. (1.5×10^7 M^{-1} s^{-1}) from β-carotene

(1) Review: *Singlet Oxygen*; Frimer, A. A., Ed.; CRC: Boca Raton, FL, 1985; Vol. I-III.
(2) (a) Gu, C.-L.; Foote, C. S.; Kacher, M. L. *J. Am. Chem. Soc.* **1981**, *103*, 5949; (b) Liang, J.-J.; Gu, C.-L.; Kacher, M. L.; Foote, C. S. *J. Am. Chem. Soc.* **1983**, *105*, 4717.
(3) (a) Ando, W.; Kabe, Y.; Miyazaki, H. *Photochem. Photobiol.* **1980**, *31*, 191. (b) Akasaka, T.; Kako, M.; Sonobe, H.; Ando, W. *J. Am. Chem. Soc.* **1988**, *110*, 494. (c) Jensen, F.; Foote, C. S. *J. Am. Chem. Soc.* **1987**, *109*, 1478.
(4) Schaap, A. P.; Recher, S. G.; Faler, G. R.; Villasenor, S. R. *J. Am. Chem. Soc.* **1983**, *105*, 1691.
(5) (a) Fenical, W.; Kearns, D. R.; Radlick, P. *J. Am. Chem. Soc.* **1969**, *91*, 7771. (b) Foote, C. S.; Fujimoto, T. T.; Chang, C. C. *Tetrahedron Lett.* **1972**, 45. (c) Hasty, N. M.; Merkel, P. B.; Radlick, P.; Kearns, D. R. *Ibid.* **1972**, 49.
(6) (a) Wasserman, H. H.; Saito, I. *J. Am. Chem. Soc.* **1975**, *97*, 905. (b) Adam, W.; Hass, W.; Sieker, G. *J. Am. Chem. Soc.* **1984**, *106*, 5020.
(7) For example, see: (a) Turner, J. A.; Herz, W. *J. Org. Chem.* **1977**, *42*, 1657. (b) Burns, P. A.; Foote, C. S.; Mazur, S. *J. Org. Chem.* **1976**, *41*, 899.
(8) (a) Foote, C. S.; Peters, J. W. *IUPAC Congr., 23rd, Spec. Lect.* **1971**, *4*, 129. (b) Monroe, B. M. *Photochem. Photobiol.* **1979**, *29*, 761. (c) Kacher, M. L.; Foote, C. S. *Photochem. Photobiol.* **1979**, *29*, 765. (d) Sawaki, Y.; Ogata, Y. *J. Am. Chem. Soc.* **1981**, *103*, 5947. (e) Akasaka, T.; Yabe, A.; Ando, W. *J. Am. Chem. Soc.* **1987**, *109*, 8085. (f) Jensen, F.; Foote, C. S. *J. Am. Chem. Soc.* **1988**, *110*, 2368.
(9) An acridine solution was pulsed at 355 nm with a Nd/YAG laser, and the data were analyzed by the Guggenheim method.[10] For experimental details, see: Ogilby, P. R.; Foote, C. S. *J. Am. Chem. Soc.* **1983**, *105*, 3423.

0002-7863/89/1511-1909$01.50/0